



Progressive damage behaviour of RTM-made composite T-joint under tensile loading

Jiang-Bo Bai^{a,*}, Chen-Hao Dong^a, Jun-Jiang Xiong^{a,**}, Chu-Yang Luo^b, Di Chen^a

^a School of Transportation Science and Engineering, Beihang University, Beijing, 100191, People's Republic of China

^b Luoyang Optoelectro Technology Development Center, Luoyang, 471009, People's Republic of China

ARTICLE INFO

Keywords:

Composites
T-joint
Progressive damage
Tensile loading
Mixed criterion

ABSTRACT

The paper deals with mechanical behaviour of the RTM (resin transfer moulding)-made composite T-joints under tensile loading. Initial failure and damage evolution behaviors as well as the load-displacement curves were determined by experiments. Progressive damage models (PDMs) of composite T-joint were presented based on the Hashin, Chang-Chang, Hou criteria and the mixed criterion, and the results predicted from the aforementioned PDMs were compared with experimental data, demonstrating the better correlation with the experiments for the predictions from the mixed criterion than from other criteria. The reason for this is that the interlaminar delamination failure can be identified and isolated by the mixed criterion. Using the PDM based on mixed criterion, the predicted initial and final failure loads have a good agreement with experiments, and the effects of triangular fillers and radius of boundary angle were investigated and discussed on initial failure loads of composite T-joint. The findings in this work are helpful to improve mechanical behaviour of composite T-joint.

1. Introduction

Composite structures (e.g. joints, stiffened panels, wing box, blades etc.) are widely used in engineering field due to excellent mechanical behaviour and ultra-light-weight [1–10]. However, composite joints are usually the weak link parts in composite structures. Thus, it is important to understand failure mechanism and mechanical behaviour of composite joints in engineering design. Experiment and finite element (FE) method are available to deal with the previous problems. Fan et al. [11] experimentally investigated failure mechanism of composite π joints under bending load, and the results showed that the delamination was the dominant failure mode of composite π joints. Fu et al. [12] conducted three-point bending tests to examine flexural properties and failure process of composite I- and π -beams, and simulated progress damage process of composite beams using a progress damage model. Luo et al. [13] also experimentally determined failure progress of composite T-joints subjected to tensile and compression loadings. Wu et al. [14] simulated progressive failure process of composite T-joints under tensile loading, and the numerical results agreed well with the experiments. Bai et al. [1] developed a progress damage model of composite π -joints under four-point flexure using the mixed criterion for simulating the damage process with an acceptable

precision. Baldi et al. [15] numerically simulated damage propagation in the adhesive interlaminar layers of composite T-joints. The predicted results correlated well with the experiments. Li et al. [16] measured mechanical properties of composite T-joints with three-dimensional four directional braided composite fillers, and found that the filler area was the weak link part of composite T-joints. Thawrel et al. [17] determined the S–N curve of composite T-joint, and predicted fatigue life of T-joint by using linear damage accumulation theory. The predicted results of fatigue life agreed well with the experimental data.

From the aforementioned reviews, it is obvious that the interlaminar properties have an appreciable influence on mechanical behaviour of composite T-joints and the interlaminar delamination is usually the dominant failure mode. In general, the interlaminar properties of composite T-joints are improved by using z-pin strengthening, ply angle design, geometrical configuration optimization, etc. Li et al. [18] investigated the influence of thickness ratio between the flange and the skin in composite T-joints on the reinforcing effect of z-pin. It was found that the z-pin could effectively improve the load-carrying capacities of composite T-joints only for the greater thickness ratio than 0.32. Nanayakkara et al. [19] revealed the effect of strengthening and toughening of volume content of z-pins on mechanical properties of

* Corresponding author.

** Corresponding author.

E-mail addresses: baijiangbo@buaa.edu.cn (J.-B. Bai), jjxiong@buaa.edu.cn (J.-J. Xiong).

<https://doi.org/10.1016/j.compositesb.2018.12.069>

Received 21 July 2018; Received in revised form 15 December 2018; Accepted 15 December 2018

Available online 17 December 2018

1359-8368/ © 2018 Elsevier Ltd. All rights reserved.

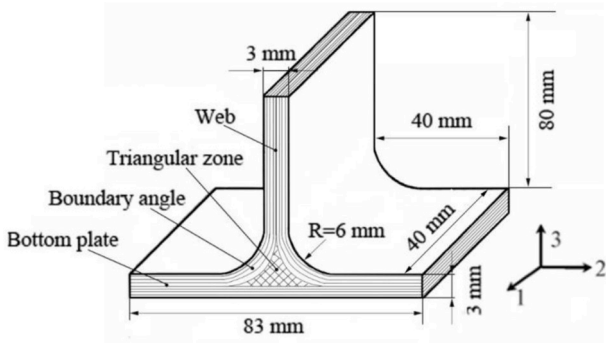


Fig. 1. Geometry and dimension of composite T-joint.

sandwich composite T-joints, and found that fracture load and fracture energy increased with the increasing volume content of z-pins. The primary toughening mechanism for pinned composite T-joints was elastic deformation, debonding and pull-out of pins from the face skins into the sandwich composite. Kim et al. [20] presented a new stitching method to improve through-thickness strength of composites. The results showed that composite T-joints made from the new method had larger failure load as against those from traditional methods. Cen et al. [21] proposed a new adhesive joint between two GFRP foam sandwich panels and investigated failure mode of new joint under four-point flexure. Bigaud et al. [22] investigated mechanical behaviour of composite T-joints reinforced by one side stitching. It was found that the stitched composite T-joints have greater ultimate strength than the unstitched ones. Burns et al. [23,24] optimized ply angle according to the arrangement of tree fibre to improve composite T-joints under bend

loading. The tensile strength was improved for optimized composite T-joints as compared with conventional ones. Hazimeh et al. [25] demonstrated the influence of ply orientation on the shear stress in the adhesive layer of composite double-lap joints under in-plane impact loading. It was reported that the shear stress in the adhesive layer was mainly influenced by the closest plies. Akpınar et al. [26] analyzed the effect of embedded supports on mechanical properties of composite T-joints using FE and experimental methods. It was involved that load-carrying capacity of composite T-joints with embedded supports had a significant improvement, but the bending stiffness had a certain reduction. Trask et al. [27] compared load-carrying abilities of composite T-joints with the same external geometry but different triangular zone area. They elucidated that the strength of composite T-joints reduced by 33% in case that the triangular zone area decreased by 50%, and the reduction of area should be tolerated within certain limits. Domingues et al. [28] investigated failure strengths of composite L-joints with different geometric dimensions and adhesives under peeling loading. It was shown that the adhesive ductility and plate thickness were important factors to affect the strength of composite L-joints. Park et al. [29] reported the combined effect of environment and manufacturing method on the strength of single-lap bonded joints, and pointed out that co-cured composite joints had the greatest strength. Cheng et al. [30] compared the influence of manufacturing process on mechanical behaviour of cross-joints made by resin transfer moulding (RTM), stitch-RTM and co-bonded techniques, and found that the RTM-made cross joints had a better mechanical property than those made by other two methods.

From the previous reviews, it is obvious that appropriate structural design and optimization as well as manufacturing process are available to improve mechanical properties of composite joints in engineering application [7]. However, it is important and essential for appropriate

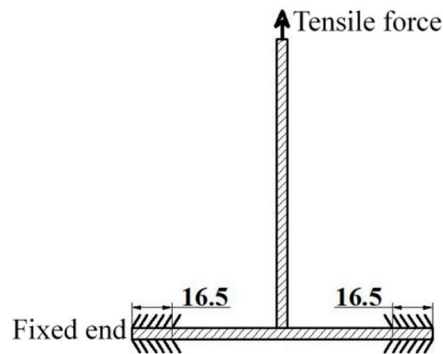


Fig. 2. Tensile test.

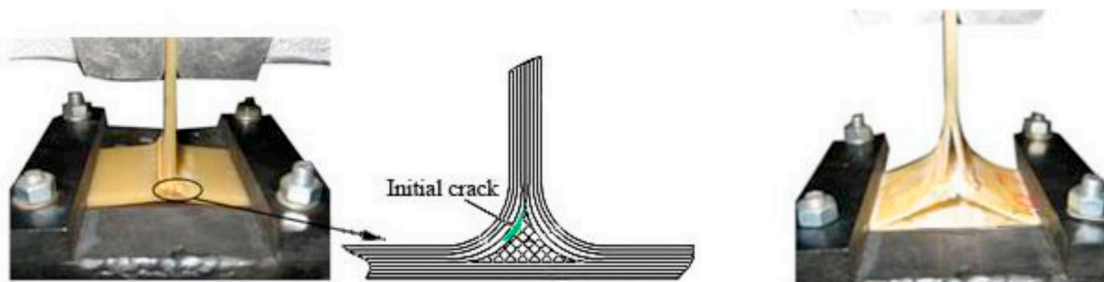


Fig. 3. Failure sequence of composite T-joint under tensile loading.

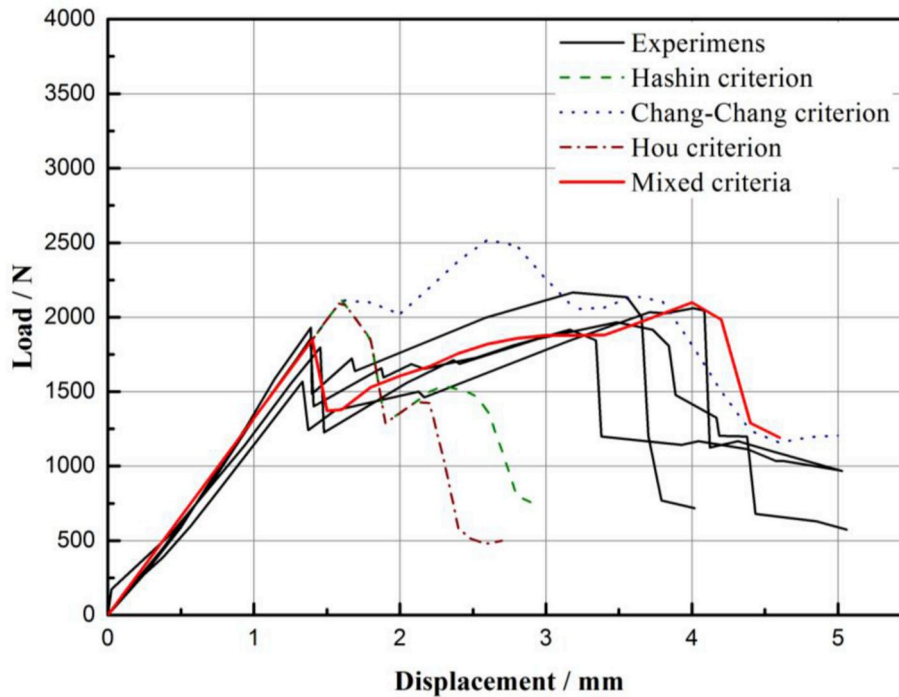


Fig. 4. Load versus displacement curves of composite T-joint under tensile loading.

Table 1
Experimental results of initial and ultimate failure loads.

	Initial failure load (N)	Final failure load (N)
Experiments	1934 1845 1567 1803	2166 1916 2061 1966
Average value of experiments	1787	2027
Prediction from mixed criterion	1850	1987
Relative deviation	3.5%	1.9%
Prediction from Hashin criterion	2114	N.A.
Relative deviation	18.3%	N.A.
Prediction from Chang-Chang criterion	2114	N.A.
Relative deviation	18.3%	N.A.
Prediction from Hou criterion	2114	N.A.
Relative deviation	18.3%	N.A.

Here relative deviation = $\frac{|\text{Mean value of experiments} - \text{Prediction}|}{\text{Mean value of experiments}} \times 100\%$

structural design and optimization to fully understand failure mechanism and mechanical properties of composite joints by using experimental method and FE analysis. Owing to the resource constraints, the progressive damage modeling (PDM) have received much interest over the last decades to simulate failure mechanism, and to predict mechanical properties of composite joints. However, there is a need for a more practical and expedient PDM technique for the application in composite structure design, which is the focus of this paper. This paper, therefore, makes an effort to provide an insight into the practical and

expedient PDM technique to exactly simulate failure mechanism and mechanical properties of composite T-joints.

2. Progressive damage analysis

2.1. Experiment

Composite T-joint specimens were made of EW220/5284 composites (i.e. EW220 glass fibre fabric and 5284 epoxy resin) and

Table 2
Mechanical properties of EW220/5284 TWF ply.

Property	Value
Longitudinal elastic modulus E_1 /GPa	14.2
Transverse elastic modulus E_2 /GPa	19.3
Through-thickness elastic modulus E_3 /GPa	5
Poisson's ratio ν_{12}	0.15
Poisson's ratio ν_{13}	0.01
Poisson's ratio ν_{23}	0.01
In-plane shear modulus G_{12} /GPa	4.3
Inter-laminar shear modulus G_{13} /GPa	3.0
Inter-laminar shear modulus G_{23} /GPa	3.0
Ply thickness/mm	0.17
Longitudinal tensile strength X_{1t} /MPa	380
Transverse tensile strength X_{2t} /MPa	493
Through-thickness tensile strength X_{3t} /MPa	50
Longitudinal compressive strength X_{1c} /MPa	312
Transverse compressive strength X_{2c} /MPa	417
Through-thickness compressive strength X_{3c} /MPa	199
In-plane shear strength X_{12} /MPa	111
Inter-laminar shear strength X_{13} /MPa	25
Inter-laminar shear strength X_{23} /MPa	30

Table 3
Mechanical properties of 5284 epoxy resin.

Property	Value
Tensile strength X_t /MPa	80
Compressive strength X_c /MPa	199.1
Elastic modulus E /GPa	3.4
Poisson's ratio	0.3

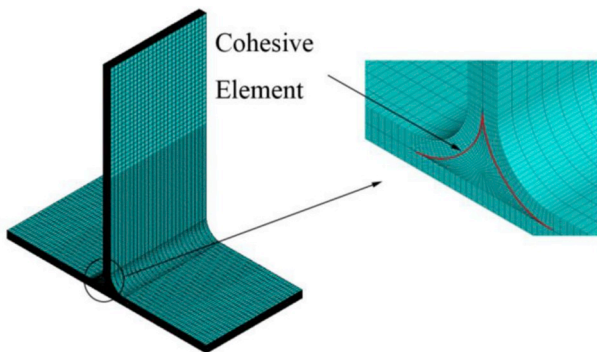


Fig. 5. FE model of composite T-joint.

Table 5
Mixed criterion.

Failure modes	Failure criterion
0° fiber breakage in tension [31]	$\frac{\sigma_1^2}{X_{1t}^2} + \frac{\tau_{12}^2}{X_{12}^2} \geq 1 (\sigma_1 \geq 0)$
0° fiber breakage in compression [31]	$\frac{\sigma_1^2}{X_{1t}^2} \geq 1 (\sigma_1 < 0)$
90° fiber breakage in tension [31]	$\frac{\sigma_2^2}{X_{2t}^2} + \frac{\tau_{12}^2}{X_{12}^2} \geq 1 (\sigma_2 \geq 0)$
90° fiber breakage in compression [31]	$\frac{\sigma_2^2}{X_{2t}^2} \geq 1 (\sigma_2 < 0)$
Fiber-matrix shear debonding [31]	$\frac{\sigma_1^2}{X_{1c}^2} + \frac{\tau_{12}^2}{X_{12}^2} + \frac{\tau_{13}^2}{X_{13}^2} \geq 1 (\sigma_2 < 0)$
Delamination failure [31]	$\frac{\sigma_3^2}{X_{3t}^2} + \frac{\tau_{13}^2}{X_{13}^2} + \frac{\tau_{23}^2}{X_{23}^2} \geq 1 (\sigma_3 \geq 0)$
Matrix cracking in tension	$\frac{\sigma}{X} \geq 1 (\sigma \geq 0)$
Matrix cracking in compression	$\left \frac{\sigma}{Y} \right \geq 1 (\sigma < 0)$
Initial interface delamination	$\left(\frac{\sigma_{II}}{\sigma_{II}^0} \right)^2 + \left(\frac{\sigma_{III}}{\sigma_{III}^0} \right)^2 + \left(\frac{\tau}{\tau^0} \right)^2 = 1$
Interface delamination propagation [34]	$G_{equic} = G_{IC} + (G_{IIC} - G_{IC}) \left(\frac{G_{II} + G_{III}}{G_I + G_{II} + G_{III}} \right)^\eta$

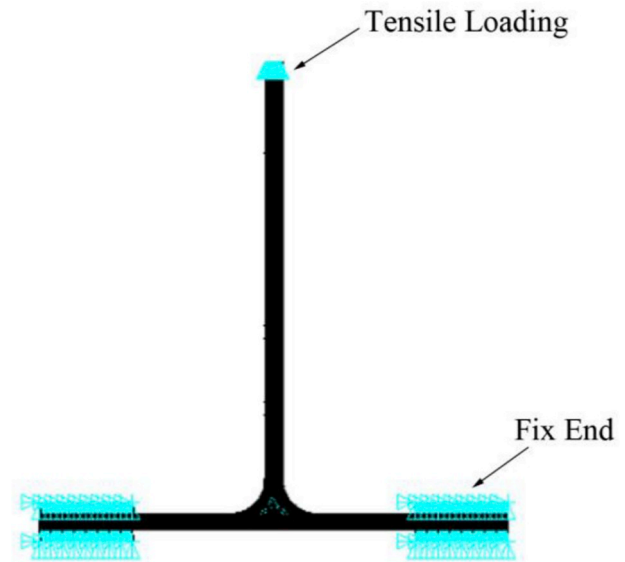


Fig. 6. Load and boundary condition.

Table 4
Mechanical properties of cohesive element.

G_{IC} (kJ/m ²)	G_{IIC} (kJ/m ²)	σ_n^0 (MPa)	τ_t^0 (MPa)	τ_s^0 (MPa)
1.5026	0.89	20	23	23

manufactured using the RTM technique [12]. Fig. 1 shows the geometry and dimensions of composite T-joint with 83 mm length, 83 mm height, 40 mm width, 6 mm boundary angle radius, 3 mm bottom plate thickness and 6 mm web thickness.

The experiment was conducted on a MTS880-100 kN servo-hydraulic machine at a displacement rate of 3 mm/min in a dry state at

Table 6
Degradation rules for material properties.

Failure mode	Degradation rule
90° fiber breakage in tension	$E_{11} = E_{22} = E_{33} = G_{12} = G_{13} = G_{23} = \nu_{12} = \nu_{13} = \nu_{23} = 0.1$
90° fiber breakage in compression	$E_{11} = E_{22} = E_{33} = G_{12} = G_{13} = G_{23} = \nu_{12} = \nu_{13} = \nu_{23} = 0.1$
0° fiber breakage in tension	$E_{11} = 0.07E_{11}$
0° fiber breakage in compression	$E_{11} = 0.07E_{11}$
Interlaminar delamination	$E_{33} = 0.01E_{33}, G_{13} = 0.01G_{13}, G_{23} = 0.01G_{23}$
Fiber-matrix shear debonding	$E_{22} = 0.8E_{22}, G_{12} = 0.8G_{12}, G_{23} = 0.2G_{23}, E_{33} = 0.2E_{33}, G_{13} = 0.2G_{13}$
Matrix cracking within triangular zone in tension	$E = \nu = 0.1$
Matrix cracking within triangular zone in compression	$E = \nu = 0.1$

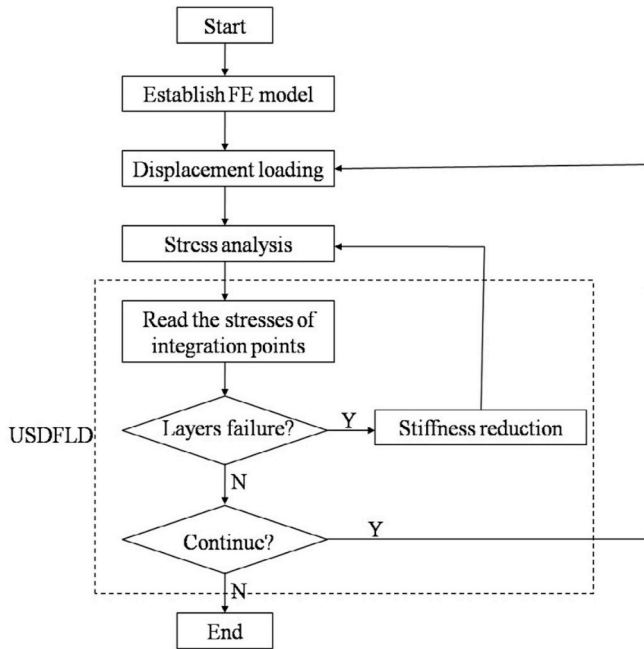


Fig. 7. Scheme flowchart of PDM using APDL routine.

room temperature. The test configuration is shown in Fig. 2. Both sides of the bottom plate in specimens were fixed and the pulling load was applied on the top of the web. The load versus displacement curves for four composite T-joints are shown in Fig. 4. The failure process captured in the experiment is shown in Fig. 3. From Fig. 3, it is clear that the delamination failure first appeared at the interface between the triangular resin-rich zone and the curved webs. This happened at a tensile load of about 1787 N (shown in Fig. 4). Then the delamination propagated along the interface to the bottom plate and spread to both sides. Still, the composite T-joint continued to carry the tension load until fiber breakage at both sides on the upper bottom plate. Experimental results of initial and ultimate failure loads for the T-joints are listed in Table 1. The mean values of experimental results of initial and ultimate failure loads for the T-joint are 1787 N and 2027 N, respectively.

2.2. Failure model of the T-joint

By means of ANSYS code, a 3D progressive damage model is established to model composite T-joint made up of the EW220/5284 plies, and the mesh model is generated on macro level of ply, rather than micro level of constituent materials (or fiber and matrix). In other words, mechanical properties of laminate elements in the PDM of T-joint are defined by ones of EW220/5284 ply, rather than constituent

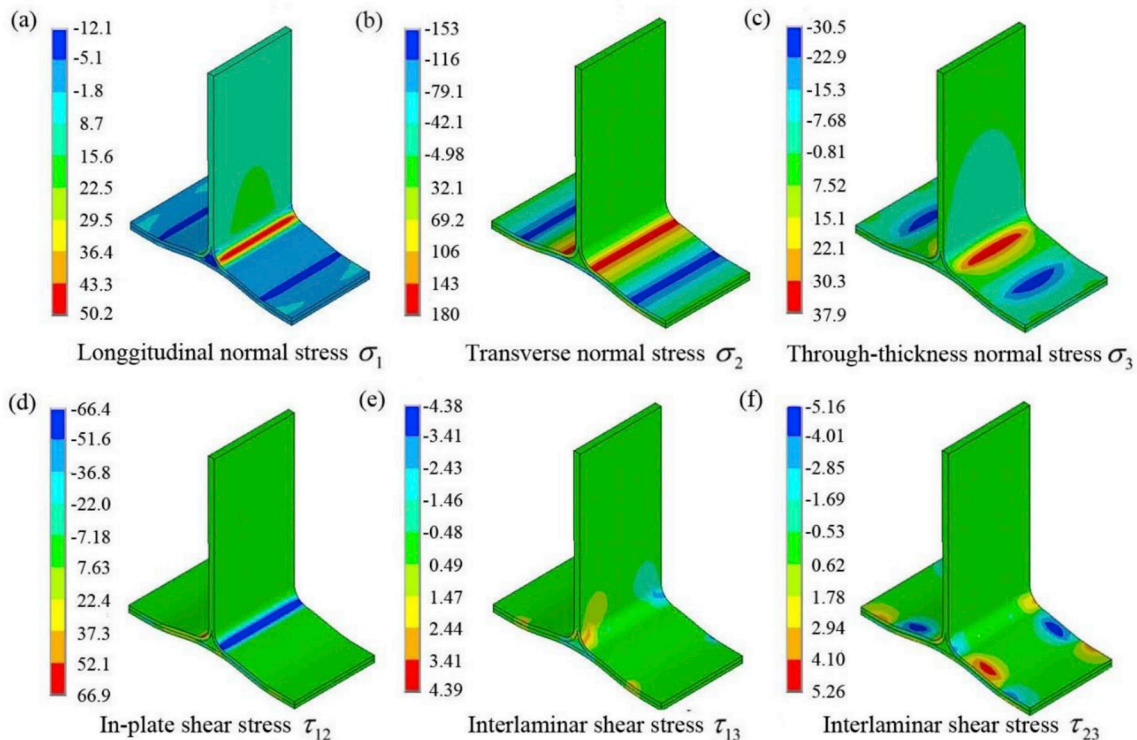


Fig. 8. Simulated stress distribution of T-joint with initial failure under tensile loading.

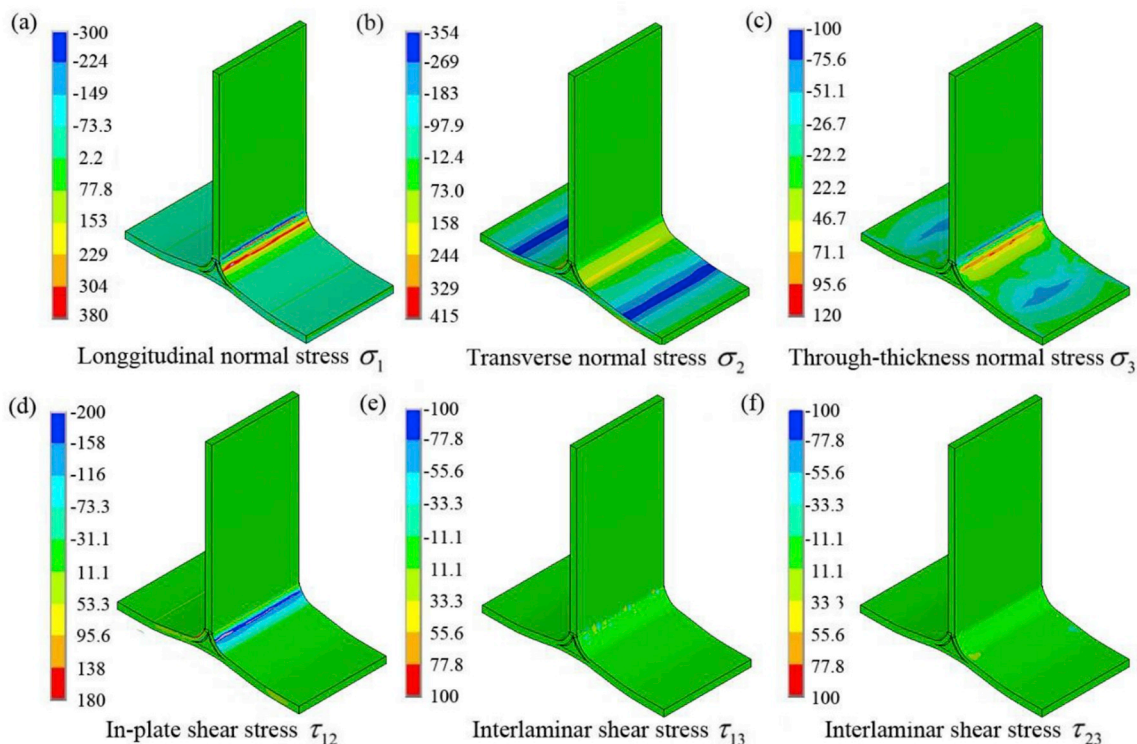


Fig. 9. Simulated stress distribution of T-joint with final failure under tensile loading.

materials. Solid element 191 is used to model composite laminate and the total number of element is 83200, mechanical properties of laminate elements are listed in Table 2. Solid element 45 is applied to simulate the matrix in triangular resin-rich zone and the total number of element is 12675, mechanical properties of matrix elements are listed in Table 3. In order to simulate the interlaminar delamination between the triangular resin-rich zone and the curved webs, cohesive elements are arranged on the interface between the triangular resin-rich zone and the curved webs (denoted by the red in Fig. 5). Interface element 204 is employed and the total number of element is 1300, mechanical properties of cohesive elements are listed in Table 4. According to the test configuration (shown in Fig. 2), boundary conditions and constraint are applied on the FE model (shown in Fig. 6). Tensile force is applied by tensile displacement loading (shown in Fig. 6) and the bottom plates are fully fixed (shown in Fig. 6). In addition, the edges and interfaces of sharp inner angles in triangular resin-rich zone are critical areas and possibly cause the irregular elements, significantly decreasing the

simulating accuracy. For this reason, the element sizes near the sharp inner angles should be numerous refined and checked until the predicted result is not sensitivity to the mesh quantity and quality.

Failure criterion and degradation rule of material stiffness play an important role in the PDM. Failure criterion is used to judge and identify the failure mode of element, and the degradation rule is applied to degrade the stiffness of failed element. A mixed failure criterion incorporating the Hashin [31], maximum stress, B–K criteria [32] and the cohesive model are implemented to identify the failures of fiber, matrix and delamination in composite T-joint (shown in Table 5), here the Hashin criterion is for isolating the fiber breakage and shear debonding between fiber and matrix, while the maximum stress and B–K criteria are used to respectively identify the matrix cracking in the triangular resin-rich zone and the interlaminar delamination propagation of the interface between triangular filler and boundary angle. The degradation rules of material stiffness corresponding to failure modes are shown in Table 6, and the PDM for composite T-joint are carried out

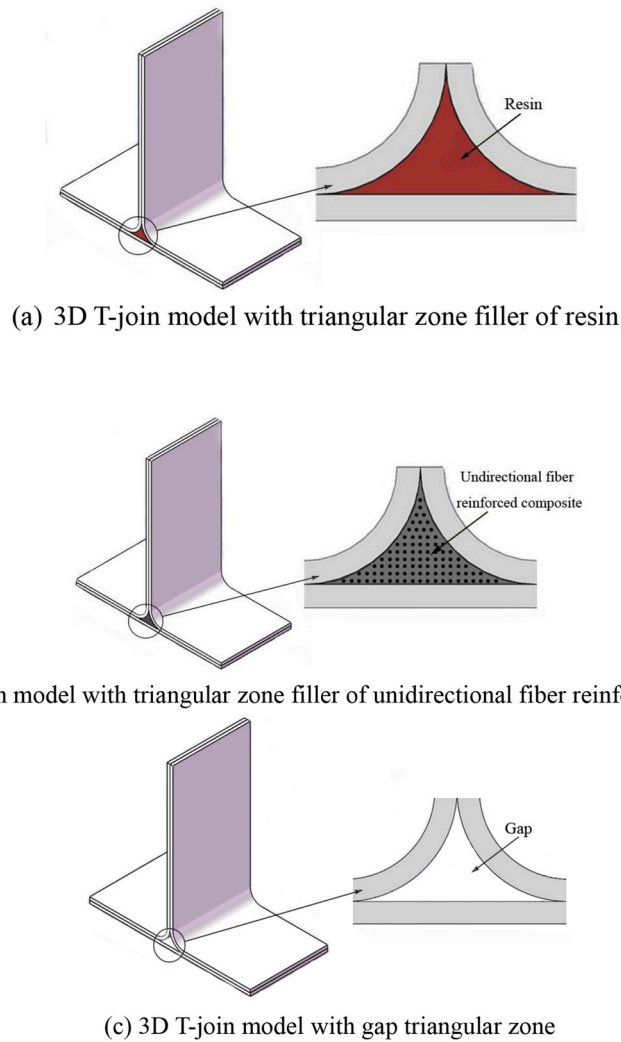


Fig. 10. 3D model of composite T-joint with different triangular zone fillers.

Table 7
Mechanical properties of unidirectional fiber reinforced composite.

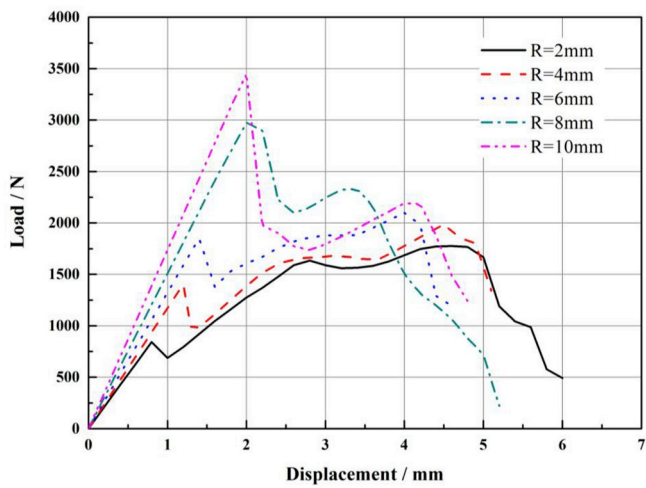
Property	Value
Longitudinal elastic modulus E_1 /GPa	47.9
Transverse elastic modulus E_2 /GPa	12.7
Through-thickness elastic modulus E_3 /GPa	12.7
Poisson's ratio ν_{12}	0.3
Poisson's ratio ν_{13}	0.3
Poisson's ratio ν_{23}	0.15
In-plane shear modulus G_{12} /GPa	4.7
Inter-laminar shear modulus G_{13} /GPa	4.7
Inter-laminar shear modulus G_{23} /GPa	3.0
Ply thickness/mm	1765
Longitudinal tensile strength X_{1t} /MPa	60
Transverse tensile strength X_{2t} /MPa	60
Through-thickness tensile strength X_{3t} /MPa	1227
Longitudinal compressive strength X_{1c} /MPa	60
Transverse compressive strength X_{2c} /MPa	60
Through-thickness compressive strength X_{3c} /MPa	135
In-plane shear strength X_{12} /MPa	86
Inter-laminar shear strength X_{13} /MPa	86

in an APDL routine (shown Fig. 7). In order to understand the effect of failure criteria on the PDM, the Hashin [31], Chang-Chang [32], Hou [33] criteria are also employed in an APDL routine.

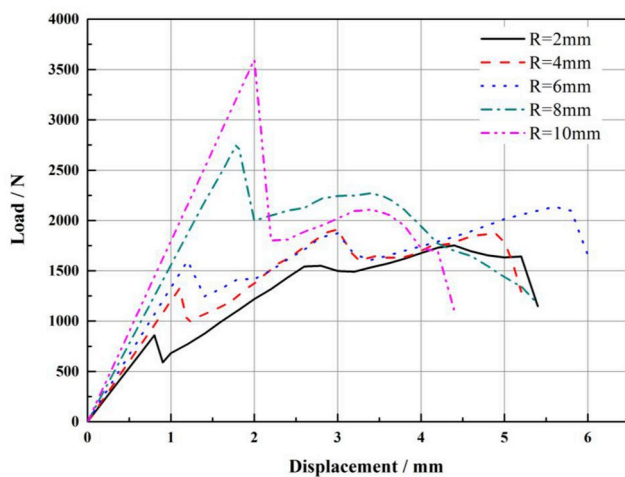
2.3. Mechanical characteristics analysis of the T-joint

The predictions for load-displacement curves and critical failure loads of composite T-joint are shown in Fig. 4 and Table 1. From Fig. 4 and Table 1, it is clear that the results predicted from the mixed criterion agree with the experiments much better than those from the Hashin, Chang-Chang and Hou criteria. The maximum relative deviations of initial and ultimate failure loads simulated by using the mixed criterion from the experiments are respectively 3.5% and 1.9%, whereas only the ultimate failure load could be predicted using the Hashin, Chang-Chang and Hou criteria and the maximum relative deviation are 18.3%. Thus, it is argued that the mixed criterion has better accuracy than the Hashin, Chang-Chang and Hou criteria in the PDM for composite T-joint under tensile loading.

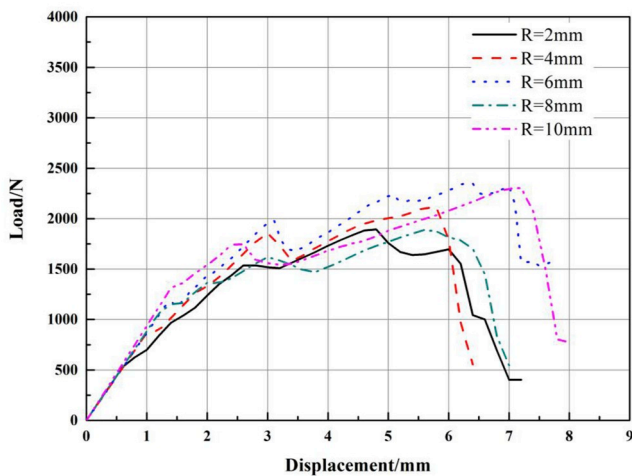
The simulations of stress pattern for the T-joint under initial and final tensile failure loading are respectively shown in Figs. 8 and 9.



(a) For triangular zone filler of resin



(b) For triangular zone filler of unidirectional fiber reinforced composite



(c) For gap triangular zone

Fig. 11. Load versus displacement curves for T-joint with different triangular zone filler.

From Figs. 8 and 9, it can be shown that severe stress concentration occurs on the interfaces between the curved webs and triangular resin-rich zone, and the through-thickness bonding strength on the interface is much lower than longitudinal and transverse strengths, hence the initial interlaminar debonding first appears on the interface between the curved webs and triangular resin-rich zone, which leads to the first load drop (shown in Fig. 4). After this, with the increase in tension loading, the interlaminar debonding spreads along the interfaces between the curved webs and triangular resin-rich zone to the bottom plate, and then the interlaminar delamination propagates along the interfaces between the curved webs and the bottom plate. Finally, the upper bottom plates (or curved webs) drastically deform upward, and immense compression stress deduces fiber breakage on the upper surface of upper bottom plate to lead to final load drop on load-displacement curve (shown in Fig. 4). The finding correlates well with the experiments.

3. Effects of triangular zone filler and boundary angle radius

From the above simulations, it is clear that the initial interlaminar debonding first appears on the interface between the curved webs and triangular resin-rich zone, and the triangular zone filler and boundary angle radius have an influence on mechanical behaviours of composite T-joint. The PDMs are generated to model composite T-joints with three different triangular zone fillers of resin, unidirectional fiber reinforced composite and gap, and five boundary angle radii of 2 mm, 4 mm, 6 mm, 8 mm and 10 mm (shown in Fig. 10). Table 7 shows mechanical properties of unidirectional fiber reinforced composite.

The simulated results for load versus displacement curves and initial failure loads are shown in Figs. 11 and 12 and Table 8. From Figs. 11 and 12 and Table 8, it can be seen that the initial failure load is the largest for composite T-joint with triangular zone filler of resin, but the lowest for one with gap triangular zone. For composite T-joint with the same triangular zone filler, the initial failure load increases with the increase in boundary angle radius. Therefore, the PDMs based on the mixed criterion in this paper is argued to be capable of evaluating mechanical behaviours of composite jointed structures subjected to static loading only from the material properties of ply and structural geometrical dimensions.

4. Conclusion

This paper seeks to investigate mechanical behaviours and failure mechanism of composite T-joint under tensile loading by using the PDMs, and to evaluate the influence of failure criterion on the predictions of mechanical behaviours. Significant results emerging from the investigations are as follows:

- (1) The PDM based on the mixed criterion presented in this paper has better accuracy than those from the Hashin, Chang-Chang and Hou criteria for predicting mechanical behaviors of composite T-joint under tensile loading. The maximum relative deviations of initial and ultimate failure loads simulated by using the mixed criterion from the experiments are respectively 3.5% and 1.9%.
- (2) Triangular zone filler and boundary angle radius have significant influence on mechanical behaviors of composite T-joint under tensile loading, and composite T-joint with triangular zone filler of resin can obtain the better tensile properties by adjusting an appropriate boundary angle radius.

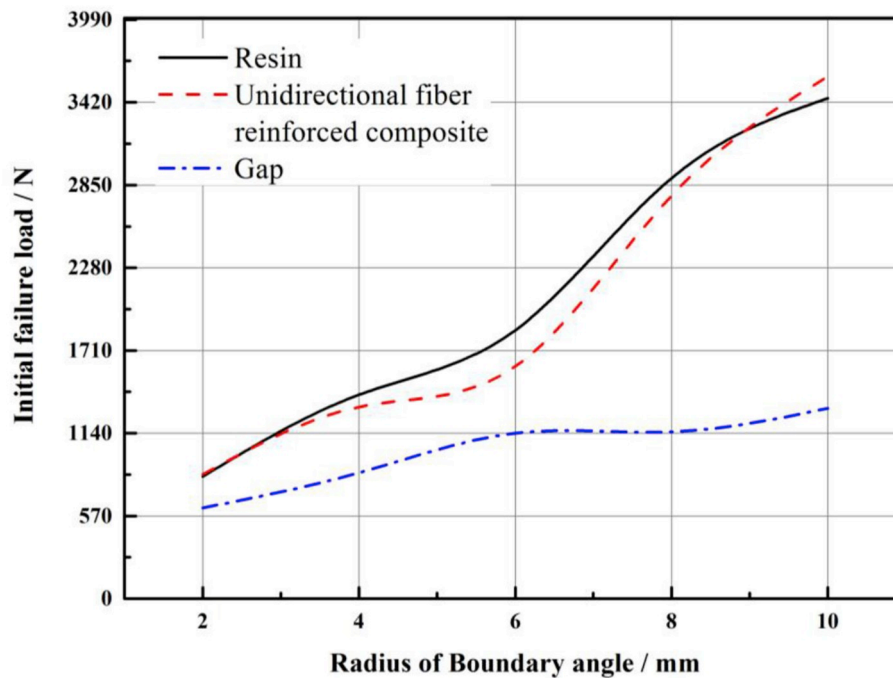


Fig. 12. Initial failure load versus boundary angle radius curves of composite T-joint.

Table 8

Initial failure loads for composite T-joint.

Radius of boundary angle/ mm	Initial failure load/N		
	Resin	Unidirectional fiber reinforced composite	Gap
2	842	858	625
4	1405	1321	868
6	1850	1600	1140
8	2897	2776	1150
10	3448	3599	1312

Acknowledgements

This project was supported by the National Natural Science Foundation of China (Grant Nos. 51875026 and 51875021).

Appendix A. Supplementary data

Supplementary data to this article can be found online at <https://doi.org/10.1016/j.compositesb.2018.12.069>.

References

[1] Bai JB, Shenoi RA, Yun XY, Xiong JJ. Progressive damage modelling of hybrid RTM-made composite P-joint under four-point flexure using mixed failure criteria. *Compos Struct* 2017;159:327–34.

[2] Zhao L, Gong Y, Qin T, Mehmood S, Zhang J. Failure prediction of out-of-plane woven composite joints using cohesive element. *Compos Struct* 2013;106:407–16.

[3] Bai JB, Chen D, Xiong JJ, Shenoi RA. A corrugated flexible composite skin for morphing applications. *Compos B Eng* 2017;131:134–43.

[4] Bai JB, Xiong JJ, Gao JP, Yi XS. Analytical solutions for predicting in-plane strain and interlaminar shear stress of ultra-thin-walled lenticular collapsible composite tube in fold deformation. *Compos Struct* 2013;97:64–75.

[5] Wang Z, Bai JB, Sobey A, Xiong JJ, Shenoi RA. Optimal design of triaxial weave fabric composites under tension. *Compos Struct* 2018;201:616–24.

[6] Xiong JJ, Shenoi RA. General aspects on structural integrity. *Chin J Aeronaut*. in press. <http://doi.org/10.1016/j.cja.2018.07.18>.

[7] Deng XW, Wu N, Yang K, Chan WL. Integrated design framework of next-generation 85-m wind turbine blade: modelling, aeroelasticity and optimization. *Compos B Eng* 15 February 2019;159:53–61 <https://doi.org/10.1016/j.compositesb.2018.09.028>.

[8] Bazilevs Y, Korobenko A, Deng X, Yan J. Fluid–structure interaction modeling for

fatigue-damage prediction in full-scale wind-turbine blades. *J Appl Mech* 2016;83(6):061010.

[9] Deng X, Korobenko A, Yan J, Bazilevs Y. Isogeometric analysis of continuum damage in rotation-free composite shells. *Comput Methods Appl Mech Eng* 2015;284:349–72.

[10] Bazilevs Y, Deng X, Korobenko A, Scalea FL, Todd MD, Taylor SG. Isogeometric fatigue damage prediction in large-scale composite structures driven by dynamic sensor data. *J Appl Mech* 2015;82(9):091008.

[11] Fan JF, ChengXQ, Wang SW, et al. Experimental and numerical investigation of composite bolted p-joint subjected to bending load. *Compos B Eng* 2015;78:324–30.

[12] Fu Y, Xiong JJ, Luo CY, et al. Static mechanical properties of hybrid RTM-made composite I- and P-beams under three-point flexure. *Chin J Aeronaut* 2015;28(3):903–13.

[13] Luo CY, Xiong JJ. Static pull and push bending properties of RTM-made TWF composite tee-joints. *Chin J Aeronaut* 2012;25(2):198–207.

[14] Wu H, Xiao JY, Xing SL, et al. Numerical and experimental investigation into failure of T700/bismaleimide composite T-joints under tensile loading. *Compos Struct* 2015;130:63–74.

[15] Baldi A, Airoldi A, Crespi M, et al. Modelling competitive delamination and debonding phenomena in composite T-Joints. *Proc Eng* 2011;10:3483–9.

[16] Li XK, Lin ZG, Hu L, et al. Numerical investigation of T-joints with 3D four directional braided composite fillers under tensile loading. *Appl Compos Mater* 2017;24:171–91.

[17] Thawre MM, Pandey KN, Dubey A, et al. Fatigue life of a carbon fiber composite T-joint under a standard fighter aircraft spectrum load sequence. *Compos Struct* 2015;127:260–6.

[18] Li MJ, Chen PH, Kong B, et al. Influences of thickness ratios of flange and skin of composite T-joints on the reinforcement effect of Z-pin. *Compos B Eng* 2016;97:216–25.

[19] Nanayakkara AM, Feih S, Mouritz AP. Improving the fracture resistance of sandwich composite T-joints by z-pinning. *Compos Struct* 2013;96:207–15.

[20] Hun J, Kweon JH, Choi JH. Fatigue characteristics of stainless steel pin-reinforced composite hat joints. *Compos Struct* 2014;108:49–56.

[21] Cen B, Liu Y, Zeng Z, et al. Mechanical behavior of novel GFRP foam sandwich adhesive joints. *Compos B Eng* 2017;130:1–10.

[22] Bigauda J, Aboura Z, Martins AT, et al. Analysis of the mechanical behavior of composite T-joints reinforced by one side stitching. *Compos Struct* 2018;184:249–55.

[23] Burns LA, Mouritz AP, Pook D, et al. Strength improvement to composite T-joints under bending through bio-inspired design. *Compos Appl Sci Manuf* 2012;43(11):1971–80.

[24] Burns L, Mouritz AP, Pook D, et al. Bio-inspired hierarchical design of composite T-joints with improved structural properties. *Compos B Eng* 2015;69:222–31.

[25] Hazimeh R, Othman R, Khalil K. Influence of plies' orientations on the stress distribution in adhesively bonded laminate composite joints subjected to impact loadings. *Compos Struct* 2016;152:654–64.

[26] Akpınar S, Aydin MD, Temiz S, et al. 3-D non-linear stress analysis on the adhesively bonded T-joints with embedded supports. *Composites Part B* 2013;53:314–23.

[27] Trask RS, Hallett SR, Helenon FMM, et al. Influence of process induced defects on

- the failure of composite T-joint specimens. *Compos Appl Sci Manuf* 2012;43(4):748–57.
- [28] Domingues NRE, Trojan JC, Campilho RDSG, et al. Strength and failure modes of single-L adhesive joints between aluminium and composites. *Ciência & Tecnologia dos Materiais* 2017;29(1):e114–8.
- [29] Park YB, Song MG, Kim JJ, et al. Strength of carbon/epoxy composite single-lap bonded joints in various environmental conditions. *Compos Struct* 2010;92(9):2173–80.
- [30] Cheng X, Xiong JJ, Peng B, et al. Mechanical properties of RTM-made composite cross-joints. *Chin J Aeronaut* 2009;22(2):211–7.
- [31] Hashin Z. Failure criteria for unidirectional fiber composites. *J Appl Mech* 1980;47:329–34.
- [32] Chang FK, Chang KY. A progressive damage model for laminated composites containing stress concentrations. *J Compos Mater* 1987;21:834–55.
- [33] Hou JP, Petrinic N, Ruiz C, et al. Prediction of impact damage in composite plates. *Compos Sci Technol* 2000;60(2):228–73.
- [34] Benzeggagh ML, Kenane M. Measurement of mixed-mode delamination fracture toughness of unidirectional glass/epoxy composites with mixed-mode bending apparatus. *Compos Sci Technol* 1996;56(4):439–49.